

In Situ Cell-by-Cell Imaging and Analysis of Small Cell Populations by Mass Spectrometry

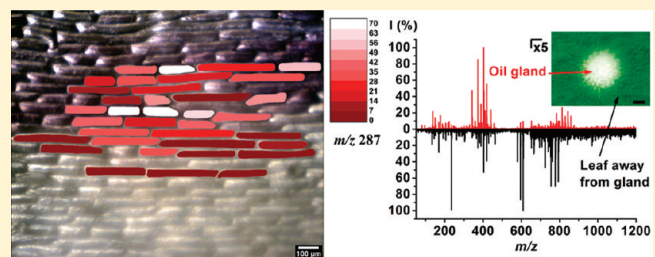
Bindesh Shrestha,[†] Joseph M. Patt,[‡] and Akos Vertes^{*,†}

[†]Department of Chemistry, W. M. Keck Institute for Proteomics Technology and Applications, The George Washington University, Washington, District of Columbia 20052

[‡]Beneficial Insects Research Unit, USDA Agricultural Research Service Subtropical Agricultural Research Center, Weslaco, Texas 78596, United States

 Supporting Information

ABSTRACT: Molecular imaging by mass spectrometry (MS) is emerging as a tool to determine the distribution of proteins, lipids, and metabolites in tissues. The existing imaging methods, however, mostly rely on predefined rectangular grids for sampling that ignore the natural cellular organization of the tissue. Here we demonstrate that laser ablation electrospray ionization (LAESI) MS can be utilized for *in situ* cell-by-cell imaging of plant tissues. The cell-by-cell molecular image of the metabolite cyanidin, the ion responsible for purple pigmentation in onion (*Allium cepa*) epidermal cells, correlated well with the color of cells in the tissue. Chemical imaging using single-cells as voxels reflects the spatial distribution of biochemical differences within a tissue without the distortion stemming from sampling multiple cells within the laser focal spot. Microsampling by laser ablation also has the benefit of enabling the analysis of very small cell populations for biochemical heterogeneity. For example, with a $\sim 30\text{ }\mu\text{m}$ ablation spot we were able to analyze 3–4 achlorophyllous cells within an oil gland on a sour orange (*Citrus aurantium*) leaf. To explore cell-to-cell variations within and between tissues, multivariate statistical analysis on LAESI-MS data from epidermal cells of an *A. cepa* bulb and a *C. aurantium* leaf and from human buccal epithelial cell populations was performed using the method of orthogonal projections to latent structures discriminant analysis (OPLS-DA). The OPLS-DA analysis of mass spectra, containing over 300 peaks each, provided guidance in identifying a small number of metabolites most responsible for the variance between the cell populations. These metabolites can be viewed as promising candidates for biomarkers that, however, require further verification.



Metabolite compositions of individual cells in a cell population differ due to gene transcription, protein expression, environmental perturbations, infection, etc.^{1–3} Flow cytometry in combination with, e.g., immunofluorescent labeling of proteins has provided insight into the heterogeneity of cells within a cell population.^{4,5} However, information related to the localization of cells in tissue is lost when these cytometry methods are used. Furthermore, once the number of cells becomes small, the analysis of the sorted cell populations becomes challenging. For example, the isolation of RNA from K-562 leukemia cells is increasingly difficult as the population size, n , reaches low ($5\,000 < n < 10\,000$) and very low ($500 < n < 1\,000$) levels.⁶ Recently, for a few selected metabolites, matrix-assisted laser desorption ionization (MALDI) mass spectrometry (MS) has also been used to study metabolic heterogeneity in microbial cultures.⁷

Chemical imaging and analysis of cell populations at atmospheric pressure by MS has broad applicability in biomedical research as well as potential for clinical diagnostics. Imaging MS has been successful at mapping proteins, lipids, and metabolites in biological tissues with molecular specificity and high sensitivity.^{8–10} Matrix-assisted laser desorption ionization (MALDI) MS has

been utilized to provide spatial distribution of neuropeptides in single neurons and analyze cell populations isolated by laser capture microdissection.^{11,12} Because of its higher spatial resolution, secondary ion mass spectrometry (SIMS) has been utilized to map chemicals at a subcellular resolution in brain tissues and membranes between fusing *Tetrahymena*.^{13,14} SIMS imaging has also been utilized to classify cancer cell lines based on statistical data reduction of their mass spectra.¹⁵ Matrix-free platforms, such as laser desorption ionization (LDI) with colloidal silver and ultraviolet LDI, have been utilized to provide MS imaging of cholesterol in individual glial cells and the distribution of secondary metabolites in *Arabidopsis thaliana*, respectively.^{16,17} In comparison to the aforementioned vacuum based methods, ambient ionization techniques offer the possibility of direct chemical mapping within biomedical specimens in their native states.^{18–20}

Received: November 14, 2010

Accepted: February 11, 2011

Published: March 09, 2011

Mapping of metabolites by MS in plant tissues at atmospheric pressure (AP) was demonstrated by AP IR-MALDI.^{21,22} Other atmospheric pressure ionization sources, such as desorption electrospray ionization (DESI) and probe electrospray ionization (PESI), were applied for the molecular imaging of animal tissue sections.^{23–25} The ability of laser ablation electrospray ionization (LAESI) MS to combine two-dimensional lateral imaging²⁶ with depth profiling²⁷ to achieve three-dimensional cross-sectional imaging²⁸ was shown in studies of rat brain and plant tissues, respectively.

In LAESI-MS, a mid-IR laser pulse of $2.94\text{ }\mu\text{m}$ wavelength is strongly absorbed by the native water content of the cell and tissue samples. The ensuing ablation ejects microscopic volumes from the sample in the form of a plume.^{29–32} Particulates in this ablated plume coalesce with the electrospray droplets and become ionized. Similar mid-IR ablation and electrospray based ionization techniques, such as IR laser-assisted desorption electrospray ionization (IR-LADESI), matrix-assisted laser desorption electrospray ionization (MALDESI), and electrospray-assisted laser desorption ionization (ELDI), have also been introduced for direct ambient analysis by MS.^{33–35}

Current imaging MS methods for the spatial mapping of molecules in tissues rely on sampling that follows a rectangular grid. The mismatch between a periodic rectangular sampling grid and the quasi-periodic cellular pattern in a tissue inevitably results in ablation spots overlapping adjacent cells. This results in the averaging of mass spectrometric signal from multiple cells leading to the loss of information on cell-to-cell compositional variations. Analysis of metabolites in a single cell by LAESI-MS can be performed by focusing the laser pulse through an etched optical fiber tip.^{36–38} In a tissue, single cells are convenient voxels for imaging because they define the natural distribution of biochemical species.

Chemometric tools based on multivariate statistics can be employed to evaluate the complex data generated in metabolomics analysis.^{39–41} Principal component analysis (PCA), a classic chemometric tool, simplifies the dimensionality of the data set by reducing the multiple variables into new variables of fewer dimensions by linear combinations.⁴² In the orthogonal projections to latent structures discriminant analysis (OPLS-DA) approach, the uncorrelated variation between the statistical variables is removed to better reveal systematic variations.^{43,44}

In this contribution, we present a novel approach for imaging MS at atmospheric pressure based on using single cells as the imaging voxels. The feasibility of cell-by-cell tissue imaging MS is demonstrated by analyzing individual cells in the *Allium cepa* tissue by LAESI-MS. The utility of multivariate statistical methods based on OPLS-DA for the extraction of biochemically distinguishing metabolites in small cell populations within the image as well as in human buccal epithelial and citrus leaf cell populations is also evaluated.

■ EXPERIMENTAL SECTION

Single-Cell LAESI-MS. Ablation in single-cell LAESI-MS analysis was produced by delivering mid-IR laser pulses through a sharpened germanium oxide-based glass optical fiber tip as described elsewhere and tabulated in Table S1 of the Supporting Information.^{36–38} Briefly, a laser pulse with 5 ns pulse width and $2.94\text{ }\mu\text{m}$ wavelength was produced by a Nd:YAG laser driven optical parametric oscillator (OPO) (Opolette 100, Opotek, Carlsbad, CA). The laser pulses were coupled into the cleaved

end of a $450\text{ }\mu\text{m}$ core diameter GeO₂-based fiber (Infrared Fiber Systems, Silver Spring, MD) by a 50 mm focal length plano-convex calcium fluoride lens (Infrared Optical Products, Farmingdale, NY). The laser pulse energies before coupling to the fiber were $0.55 \pm 0.03\text{ mJ}$. The cleaved end of the optical fiber was held by a bare fiber chuck (BFC300, Siskiyou Corporation, Grants Pass, OR) and positioned with a five-axis translator (BFT-5, Siskiyou Corporation, Grants Pass, OR). The other end of the fiber was chemically etched to produce a sharpened tip by dipping it into 1% HNO₃ (v/v) solution for ~ 15 min. The etched tip was mounted on a micromanipulator (MN-151, Narishige, Tokyo, Japan) and aligned over the cell of interest at a 45° tip angle and $\sim 30\text{ }\mu\text{m}$ from the surface. The etched tip of the fiber delivered mid-IR laser pulses to the cell causing the perforation of the cell wall and the ejection of the cell content into the ablation plume. Ablations were carried out by aiming the fiber tip at the geometric center of the cells. Delivering 20–50 laser pulses per cell ensured the sampling of a significant portion of the cell content and resulted in consistent spectra. Neutral particulates in the plume coalesced with highly charged droplets from an electrospray. The electrospray was produced by pumping 50% (v/v) aqueous methanol solution containing 0.1% (v/v) acetic acid by a low noise syringe pump (Physio 22, Harvard Apparatus, Holliston, MA) at 200 nL/min flow rate through a tapered stainless steel emitter (i.d., $50\text{ }\mu\text{m}$, MT320-50-5-5, New Objective, Woburn, MA) and by applying high voltage (2.9–3.0 kV) generated by a regulated power supply (PS350, Stanford Research Systems, Sunnyvale, CA) to it.⁴⁵ The mass spectrometer orifice-to-emitter tip distance was 12 mm, and the orifice axis-to-sample surface distance was also 12 mm. The charged droplets in the spray seeded by molecules from the sample produced corresponding positive ions that were analyzed by an orthogonal acceleration time-of-flight mass spectrometer (QTOF Premier, Waters Co., MA). The peaks in the mass spectra were assigned to metabolites based on accurate mass measurements, on matching isotope distribution patterns, on database and literature information, and, in some cases, on tandem MS measurements.

Microscopy. Visualization of the cells was required to select and target them for the LAESI-MS analysis. Two home-built long working distance microscopes were used for cell targeting and for monitoring the distance between the fiber tip and the cell surface. The former consisted of a $7\times$ precision zoom optic (Edmund Optics, Barrington, NJ), a $10\times$ infinity-corrected long working distance objective lens (M Plan Apo $10\times$, Mitutoyo Co., Kanagawa, Japan), and a CCD camera (Marlin F131, Allied Vision Technologies, Stadtroda, Germany). A similar microscope was utilized to maintain the $\sim 30\text{ }\mu\text{m}$ distance between the fiber tip and the cell surface to achieve efficient ablation without mechanically damaging the cells. This system consisted of a long distance video microscope (InFocus Model KC, Infinity, Boulder CO), a $5\times$ infinity corrected objective lens (M Plan Apo $5\times$, Mitutoyo Co., Kanagawa, Japan), and a CCD camera (Marlin F131, Allied Vision Technologies, Stadtroda, Germany).

Chemicals and Cells. HPLC grade methanol and water were purchased from Acros Organics (Geel, Belgium), and glacial acetic acid was obtained from Fluka (Munich, Germany) and used without further purification. A monolayer of cells was obtained from a purple cultivar of *A. cepa* bulbs purchased from a local market (Washington, DC). A layer of bulb scales was excised by a surgical scalpel into a strip. An intact layer of the

inner epidermal tissue was peeled away and mounted on a glass slide for LAESI-MS analysis. Human buccal mucosa epithelial cells (cheek cells) were collected from a healthy male volunteer with normal medical history by scraping the inside of the cheek after rinsing the mouth with tap water. The scraped cells were directly transferred to a clean microscope glass slide for LAESI-MS analysis. Six sour orange (*Citrus aurantium*) saplings (45 cm tall) were provided by the USDA laboratory in Weslaco, TX. The trees were maintained in a greenhouse at GWU, where they were watered twice a week with ~ 2 L of tap water and kept in natural light while awaiting analysis. Citrus leaves were excised from the plants and secured to glass slides with cellophane tape for LAESI-MS analysis.

Imaging. A three-axis translation stage (LTA-HS, Newport Corp., Irvine CA) was used to manually move the tissue sample below the fiber tip. To maintain the geometry of the LAESI-MS system, the imaging experiments were performed by moving the sample and presenting a new cell for each analysis instead of relocating the fiber tip. For each cell, ions were collected in 2 s scans, corresponding to 20 laser pulses, from the approximate center of the cell, to avoid damage to the adjacent cells. To produce comparable spectra, 5 scans were averaged from each cell. The dwell time between the analyses averaged 60 s, allowing the operator to move the sample manually. The length of the dwell time was sufficient to ensure that no cross talk occurred between the single-cell samples. A scientific visualization package, Origin (Origin 7.0, OriginLab Co., Northampton, MA), was used to produce the false color scale for the distributions of mass-selected ions, which were rendered over the optical image of the tissue through an imaging software package (Photoshop, version 7, Adobe Systems, San Jose, CA).

Data Processing. The LAESI mass spectra were obtained by subtracting the electrospray background peaks in the MassLynx 4.1 software (Waters Co., MA). Accurate alignment between the data sets was obtained by using the lock mass feature on an ion of known identity, such as the potassium sucrose ion with m/z 381.0799. Further data processing was performed with the Origin (Origin 7.0, OriginLab Co., Northampton, MA) software package on ASCII data files exported from MassLynx. Multivariate statistical data analyses, such as PCA and OPLS-DA, were performed by the Extended Statistics (XS) module that utilizes the EZinfo software (version 2.0.0.0, Umetrics AB, Sweden) within the MarkerLynx application manager (Waters Co., MA). In the statistical analyses, automatic cross validation was utilized to determine the number of components. Initially, an unsupervised multivariate statistical approach, PCA, was applied to the raw data from the mass spectrometer to identify the principal components. To identify potential biomarkers, the data was further analyzed using the supervised OPLS-DA method, with Pareto scaling. In Pareto scaling, each variable is divided by the square root of its standard deviation. The advantage of Pareto scaling over other scaling techniques is that it enhances the contribution from medium and small spectral features without inflating baseline noise or distorting spectral line shapes.^{41,46} OPLS-DA is an emerging tool for biomarker discovery in metabolomics.^{47–49} It is capable of pinpointing variables that are responsible for discrimination between groups. In this method, data belonging to different subgroups, e.g., nonpigmented cells vs pigmented cells, are compared to extract biomarkers.^{41,43,44,50} Statistically significant biomarkers are visualized by the S-plot that presents the relationship between covariance and correlation within the OPLS-DA results.^{41,43,51}

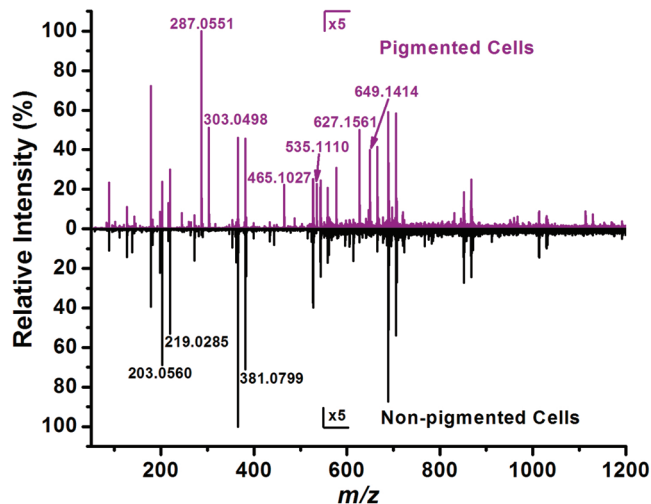


Figure 1. Positive-ion single cell LAESI mass spectra averaged over five pigmented cells (top) and five nonpigmented cells (bottom) of the *A. cepa* epidermis. The $\times 5$ magnification is applicable for both mass spectra, and the magnification starts at m/z 550.

RESULTS AND DISCUSSION

Comparative Analysis of Adjacent Cells. In order to assess the potential degradation of the surroundings of an analyzed cell, we investigated the cells immediately coordinating the ablation site. As a model system we used homogeneous tissue regions consisting of only nonpigmented epidermal cells from *A. cepa* bulbs that had been used extensively to study plant cell structures.⁵² The potential effect of cell ablation on the metabolic composition of adjacent cells was evaluated by comparing the mass spectra from single-cell analyses of adjacent cells ($n = 9$) with those of similar cells further away ($n = 9$). The same number of laser shots was used for the analysis of each cell. Hexose and disaccharide ion intensities were found to be normally distributed among similar epidermal cells in the same layer of the *A. cepa* tissue.

These experiments showed no significant difference between the cells surrounding the initial ablation site and similar cells at a distance. For example, the sodiated hexose (m/z 203) and the sodiated disaccharide (m/z 365) intensities from a single ablated cell are 521 and 246, respectively, which are within the margin of error of the average ion intensities of 456 ± 187 (RSD 41%) and 215 ± 93 (RSD 43%), respectively, obtained from the coordinating cells. The ion intensities from the cells coordinating the ablation site were similar to the average ion intensities of 582 ± 283 (RSD 49%) and 129 ± 57 (RSD 57%), respectively, measured for single cells at least 8 to 10 cells away from the original ablation site. This suggested that ablating a cell did not significantly influence the metabolic analysis of the adjacent cells. In addition, the physical integrity of cells surrounding the ablation site can be discerned from optical images.^{36,38}

The epidermal tissue in the purple *A. cepa* cultivar contains predominantly nonpigmented cells and a few patches of pigmented cells. For most cells, the difference in pigmentation observed by an optical microscope clearly distinguishes the cell populations belonging to the two phenotypes. Positive-ion mass spectra, obtained by averaging single-cell LAESI mass spectra for five pigmented ($n = 5$) and five nonpigmented ($n = 5$) cells each, are shown in Figure 1. The total acquisition time for these spectra was 100 s. A typical single cell LAESI mass spectrum contained

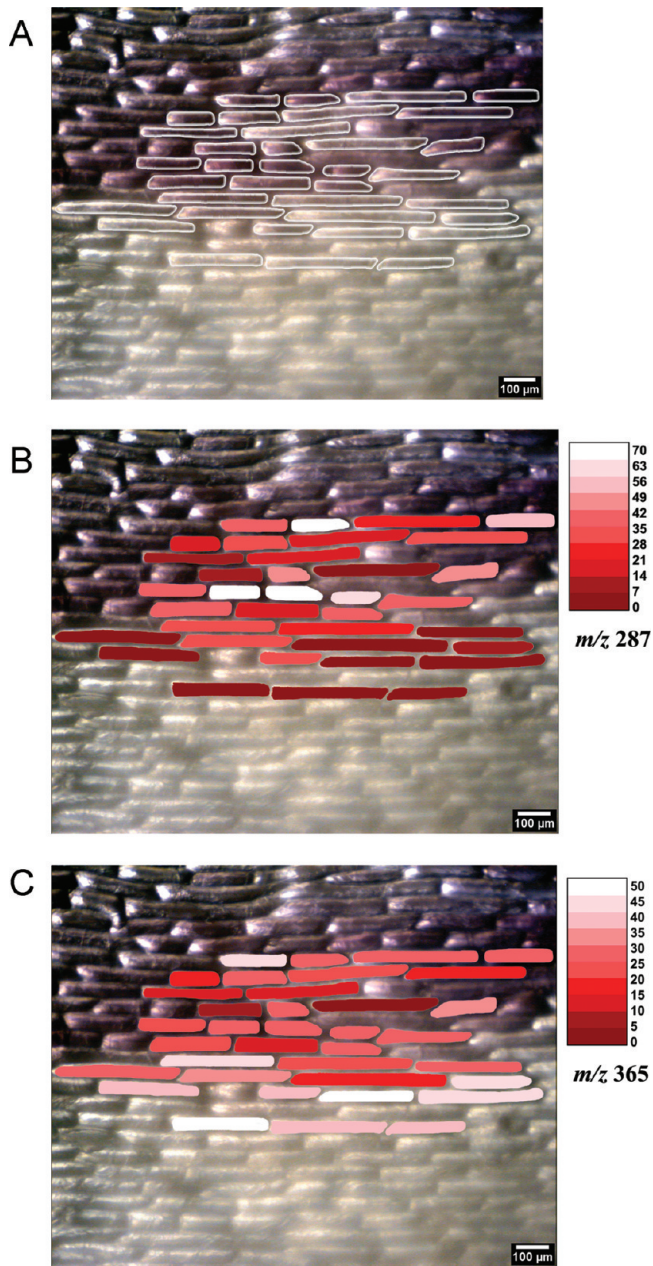


Figure 2. (A) Optical image of the studied cell population at the pigmented to nonpigmented boundary with the analyzed cells outlined. Cell-by-cell chemical images of the metabolites (B) cyanidin and (C) sucrose were created by representing the ion intensities obtained from a cell on a false color scale and coloring the corresponding cells in the optical microscope image accordingly. The chemical images show that cyanidin was selectively present in the pigmented cells ($n = 20$) whereas it was absent in the nonpigmented cells ($n = 16$) and sucrose was uniformly distributed throughout the entire studied cell population.

over 100 ions, whereas spectra averaged for multiple cells exhibited over 300 peaks. Approximately 12% of the 300 ions have been assigned. Some of the ions were sodiated or potassium adducts and for carbohydrates there were a few dimers. Most of the ions assigned ions, however, corresponded to distinct metabolites.

A direct comparison between the metabolite composition of the nonpigmented and pigmented cells in the same tissue had

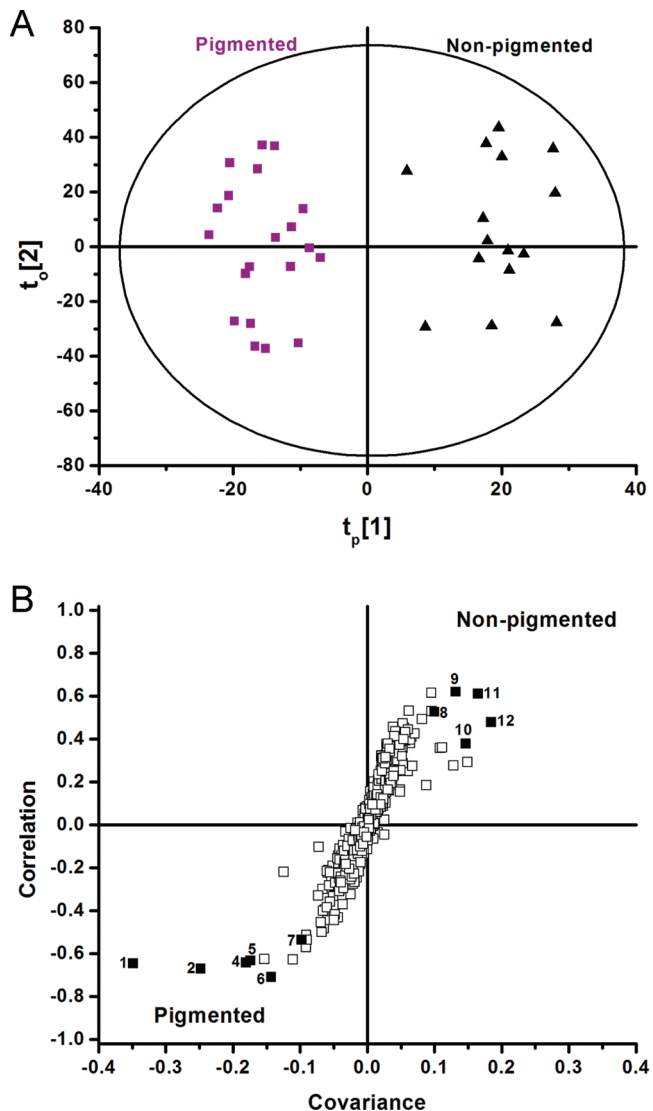


Figure 3. (A) Score plot of the OPLS-DA model completely separated the subpopulations of pigmented ($n = 20$) (purple squares) and nonpigmented cells ($n = 16$) (black triangles) in the first predictive component, $t_p[1]$, whereas the variations within the subpopulations was seen in the orthogonal component, $t_o[2]$. All the points fell well within the Hotelling T^2 range with a significance level of $p = 0.05$ represented by the ellipse, and no cells were misclassified. (B) The wings of the S-plot with the highest correlation and covariance values signify the metabolites that account for most of the variance between the two subpopulations. Selected points in the S-plot (solid squares) in comparison with Table S2 of the Supporting Information clearly indicated that cyanidin (SN = 1) and quercetin (SN = 2) are characteristic of the pigmented cells.

been reported earlier.³⁶ Compared to the nonpigmented cells, additional metabolites, such as anthocyanidins, flavonoids, and their glucosides, were present in the pigmented cells.

Cell-by-Cell Imaging. The robust mass spectrometric signal from adjacent cells suggested the feasibility of cell-by-cell imaging. LAESI-MS was utilized to perform chemical imaging at the transition between the pigmented and nonpigmented cells (see the optical image in Figure 2A). Single cells were used as voxels to demonstrate the feasibility of molecular imaging by performing successive LAESI-MS analysis on 36 cells at the nonpigmented–pigmented boundary. The chemical profile of

each single cell in the small chemical image is correlated by a mass spectrum enabling us to assess cell-by-cell metabolite distributions.

The cellular distribution of the detected metabolites was visualized by coloring each analyzed cell in the optical microscope image of the tissue based on a false color scale representing the intensity of the corresponding ion normalized for the spectrum of the given cell (see Figure 2B,C). Optical microscopy indicated the presence of the natural purple pigment, known to contain cyanidin, in the cells located in the top portion of the tissue (see Figure 2A). A good correlation between the cellular distribution of the protonated cyanidin ion and the pigmented cells is apparent in Figure 2B. Similarly, quercetin, a flavonoid, has also been found predominantly in the pigmented cells (see Figure S1a in the Supporting Information). Primary metabolites, such as sucrose, were distributed uniformly throughout all the studied cells with slightly higher intensities in the nonpigmented cells (see Figure 2C). Another metabolite alliin, a derivative of the amino acid cysteine and the precursor of allicin and other sulfur compounds responsible for the smell of onions, seemed to be highly concentrated in two of the studied cells with much lower or no alliin content in other cells (see Figure S1b in the Supporting Information). The small scale cell-by-cell chemical imaging presented here demonstrates the feasibility of using LAESI-MS for studying the distribution of metabolites, lipids, and other compounds. These results also point to the possibility to identify distinct subpopulations within seemingly similar sets of cells.

Cell Population Analysis. Multivariate statistical analysis methods, such as PCA and OPLS-DA, had been successful in the evaluation of complex metabolomics data.^{40,41} In this study OPLS-DA was utilized to identify metabolites responsible for most of the variance between LAESI mass spectra of visually distinguishable phenotypes, e.g., nonpigmented and pigmented epidermal cells of *A. cepa*. In the score plot of the OPLS-DA model, presented in Figure 3A, the subpopulations of pigmented and nonpigmented cells were completely separated in the first predictive component, $t_p[1]$, whereas the orthogonal component, $t_o[2]$, described the variation within the subpopulations. The analysis of single cells, represented by the points in this plot, fall well within the Hotelling T^2 range with a significance level of $p = 0.05$ (see the ellipse in Figure 3A), and no cells are misclassified.

The S-plot is a scatter plot that visualizes the covariance and correlation loading profiles based on the predictive component, $t_p[1]$, of the OPLS-DA model. In the S-plot, the y -axis denotes reliability of metabolite ions that contribute to the difference in the signal between the cell populations, i.e., the correlation, and the x -axis denotes the contribution magnitude of the ions to the cell population difference, i.e., the covariance. The labels in the S-plot describe which cell populations correspond to the positive and the negative axes. For example in Figure 3B, the correlation of 1 corresponds to nonpigmented cells, whereas the correlation of -1 represents pigmented cells. The wings of the S-plot with the highest correlation and covariance values signify the metabolites that account for most of the variance between the two subpopulations. Conversely, the metabolites represented by points in the center of the S-plot do not significantly contribute to the variance between the two subpopulations. In Figure 3B, most of the metabolites are found close to the center, indicating that the epidermal cell subpopulations are very similar in their metabolite composition.

With the wings of the S-plot in Figure 3B looked at, the cyanidin and quercetin ions (with serial numbers SN = 1 and SN = 2,

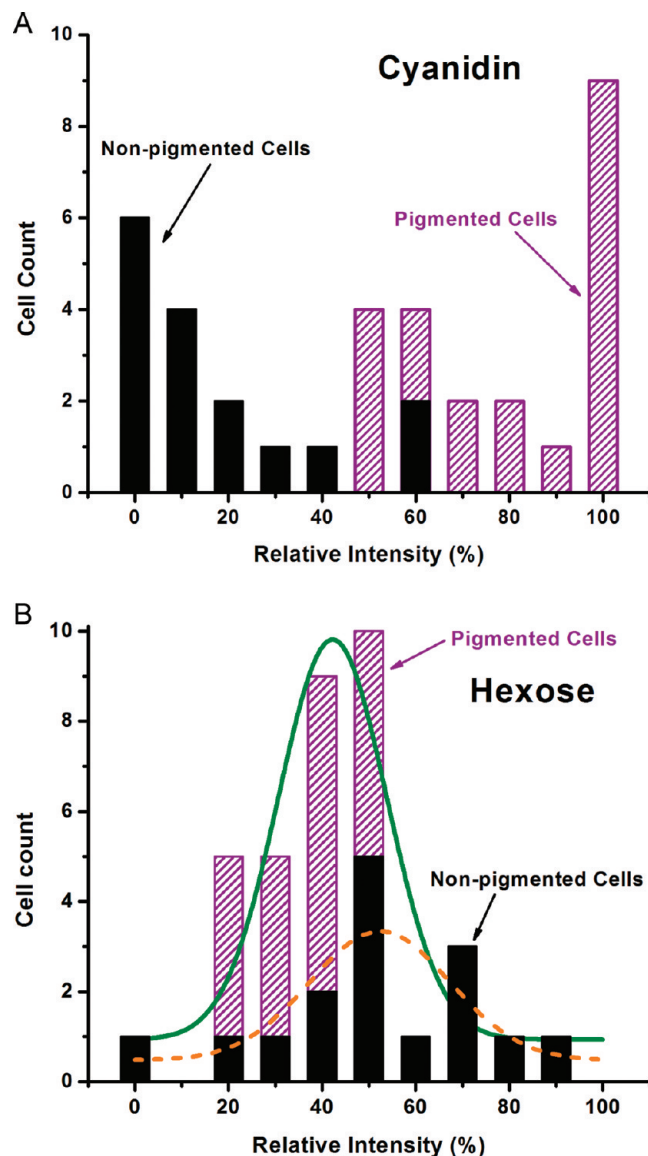


Figure 4. (A) Intensity distribution of cyanidin in the total cell population ($n = 36$) exhibits two or three maxima with the nonpigmented ($n = 16$) (solid black) and pigmented ($n = 20$) (shaded purple) cell subpopulations responsible for the low and high intensity modes, respectively. (B) The ion intensity distribution of hexose showed a single maximum with slightly higher intensity values for the nonpigmented (solid black) subpopulation. The solid green and dashed orange lines represent the Gaussian fits to the total cell population and the nonpigmented subpopulation, respectively.

respectively) were identified as the metabolites most closely associated with the pigmented cell subpopulation. This is consistent with earlier results on single *A. cepa* cells.³⁶ In contrast, the potassium hexose ($SN = 11$) and potassium disaccharide ($SN = 9$), at m/z 219 and 381, respectively, show lower covariance and correlation values indicating that these metabolites do not efficiently differentiate between the two subpopulations. Indeed, although their ion intensities are slightly higher in the nonpigmented cells, they are also present in the pigmented ones. Among the 12 metabolite ions found in the wings of the S-plot (see Table S2 in the Supporting Information), cyanidin and quercetin intensities exhibit the strongest difference in the

spectra of the two cell subpopulations. The metabolites marked by an asterisk in Table S2 are confirmed by tandem MS measurements. Numerous points are found in the center of the S-plot indicating that many of the metabolite ions are present in the two subpopulation spectra with similar abundances. In such cases, relatively few metabolites can be selected as biomarker candidates.

Comparison of Highly Dissimilar Cells. To test the OPLS-DA analysis for highly dissimilar cell populations, LAESI mass spectra were compared for nonpigmented *A. cepa* epidermal cells and human buccal mucosa epithelial cells (cheek cells). The mass spectra of buccal cells (see Figure S2a in the Supporting Information) showed the presence of small metabolites and lipids (see Table S3 in the Supporting Information for a few selected assignments). The typical LAESI mass spectrum of buccal epithelial cells significantly differs from the spectrum of *A. cepa* epidermal cells.

To identify the metabolites that account for the variance between the two cell populations, OPLS-DA was carried out on the corresponding LAESI spectra. Compared to the S-plot for the mildly dissimilar epidermal cell phenotypes shown in Figure 3B, the S-plot for these highly dissimilar cells was much more polarized. The large differences between these cells resulted in an expanded correlation range covering almost the entire -1 to 1 domain, and numerous metabolites were clustered close to these extremum values with fewer species represented in the middle (see Figure S2b in the Supporting Information). This indicates that, in case of highly dissimilar cells, more metabolites correlate strongly with their respective subpopulations and have the potential to become biomarker candidates.

Metabolite Concentration Distributions over Cell Populations. Assuming that the relative ion intensities from single cells are proportional to the corresponding metabolite concentrations, the cellular heterogeneity within a population can be quantified. Frequency distributions for significant ions, selected by using the S-plot, can be constructed to approximate the probability density of finding cells with particular metabolite concentrations. In a homogeneous cell population, the density function is typically a Gaussian, whereas in heterogeneous populations, distributions with long tails or bimodal distributions are observed.

An example for the latter is demonstrated in Figure 4A. The relative ion intensities for the cyanidin ions at m/z 287 in the studied *A. cepa* cell population were binned, and the corresponding cell counts were plotted. The resulting histogram showed a bi- or perhaps trimodal distribution indicating the strongest peaks at 0% , i.e., with the cyanidin signal below the noise level, and at 100% , representing the cells with a cyanidin base peak. As in this case we can visually distinguish the nonpigmented and the pigmented phenotypes, and their contribution to the overall distribution can be separated. Figure 4A shows the nonpigmented cell counts in solid black, whereas the pigmented cells are represented in patterned purple. The figure clearly demonstrates that the two subpopulations segregate according to their cyanidin concentration, with little overlap. Indeed, the secondary metabolite cyanidin is known to be primarily present in the pigmented cells (see Figure 2B). When the histogram is looked at, it is also apparent that measuring the average cyanidin concentration for this cell population would be misleading. On the basis of this limited data, it is unclear if the weaker maximum in the center of the histogram has physiological significance or is it the result of natural or signal fluctuations.

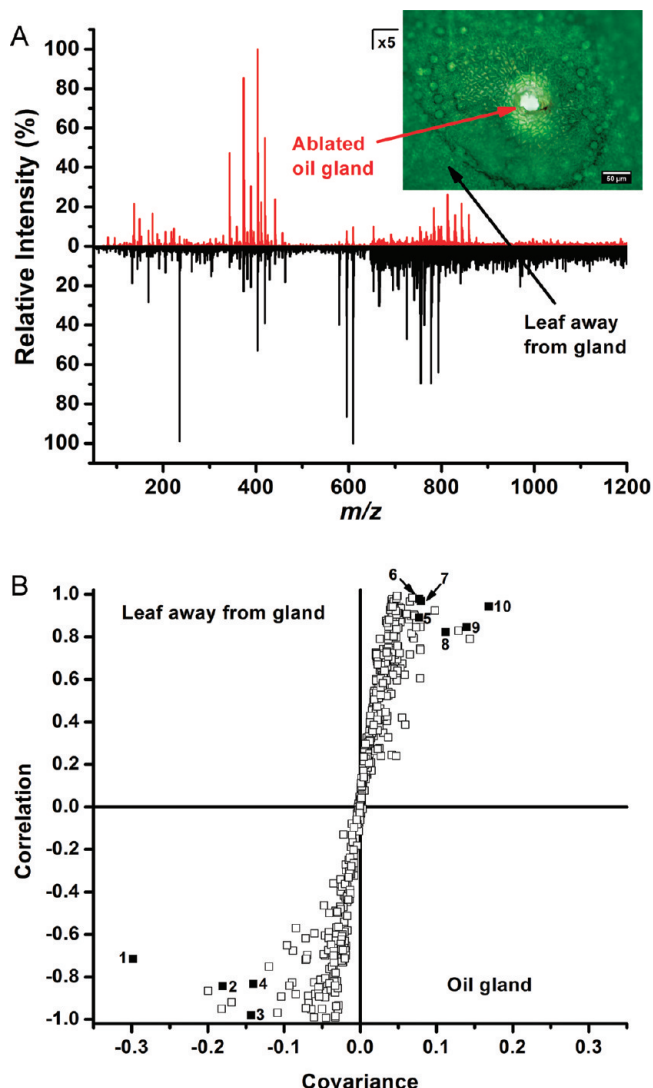


Figure 5. (A) Positive-ion LAESI mass spectra from $n = 6$ to 8 oil gland cells (pooled from the ablation of the center of two glands) of a *C. aurantium* leaf (red trace on top) and $n = 6$ to 8 cells from the leaf away from the gland (pooled from two ablation spots) (black trace in the bottom). The inset shows a microscope image of an oil gland with the ablation mark (scale bar is $50 \mu\text{m}$). The ablated spot is $\sim 30 \mu\text{m}$ in diameter. (B) S-plot produced by OPLS-DA of the spectra showed that many metabolites strongly correlated with either the oil gland cells ($n = 25$) or cells in the leaf away from the gland ($n = 25$). The 10 metabolites with serial numbers (SN) (solid squares) indicated in the figure are identified in Table S4 of the Supporting Information.

In contrast, the relative ion intensities of the primary metabolite hexose showed a broad distribution in the studied cell population with a single maximum. Figure 4B presents the corresponding histogram for the total cell population with the contribution of the two subpopulations indicated similar to Figure 4A. The solid green line represents the Gaussian fit to the total population with the center at $42 \pm 2\%$ relative hexose ion abundance and a width of $\sim 23\%$. A similar fit for the nonpigmented subpopulation indicates a slight shift to $52 \pm 5\%$ with a slightly higher width of $\sim 30\%$. Indeed, the hexose content of the two subpopulations is hardly distinguishable. The more or less uniform presence of hexoses in all the cells is

expected because they, as primary metabolites, are necessary for their functioning irrespective of the phenotype.

Biomarker Candidates in Oil Glands. Citrus leaves contain oil glands that synthesize, secrete, and store terpenoid oils.^{53,54} These organic volatiles are part of the plant defense mechanisms against herbivores. In the young leaves of *C. aurantium*, the immature glands are approximately 50 μm in size and their centers contain large achlorophyllous polyhedral cells (see the inset of Figure 5A) with \sim 15 and \sim 10 μm for the long and short axes, respectively. Within the gland they are surrounded by somewhat smaller flattened cells. Analysis of 100 μm spots would result in an average mass spectrum from the mixture of the oil gland cells, the surrounding flattened cells, and the regular epidermal cells adjacent to the gland. Although analysis of a single gland cell remains a challenge due to sensitivity limitations, LAESI-MS of the central cluster within a \sim 30 μm ablation spot is feasible. This enables the sampling and analysis of only 3 or 4 achlorophyllous cells within an oil gland.

In order to find chemical species that reliably distinguish the gland cells, local LAESI-MS analysis of $n = 6$ to 8 cells (spectra pooled from the ablation of two glands) in an oil gland of a *C. aurantium* leaf and $n = 6$ to 8 cells from the leaf away from the gland (spectra pooled from two ablation spots) was conducted. Figure 5A shows a significant difference in the obtained mass spectra. Some of the distinctive groups of biomolecules detected in the oil gland appeared to belong to terpenes and terpenoids. In contrast, LAESI-MS analysis of the epidermal cells away from the gland revealed the presence of flavonoids and common primary metabolites. Considering the low incidence of quasimolecular and cluster ions, the over 550 peaks from the spectra for the two cell types correspond to more than 400 hundred different metabolites. Some examples are listed in Table S4 of the Supporting Information, but to identify all of them would require an extraordinary amount of work. In order to concentrate our efforts on metabolites that account for most of the variance between the spectra from in and outside the glands, OPLS-DA analysis has been performed on the spectra and the obtained S-plot is displayed in Figure 5B.

Although the two cell populations reside in the same tissue, the extreme negative and positive correlation values for some metabolites approaching -1 for the oil gland and 1 for the cells away from the glands indicate that clear distinction can be made according to their localization. Identifying 10 ions in the S-plot with high correlation and covariance values (see the points with SNs in Figure 5B) enabled us to focus our efforts on the statistically most relevant metabolites. The corresponding assignments are listed in Table S4 of the Supporting Information. The metabolites marked by an asterisk in Table S2 are confirmed by tandem MS measurements. Four metabolites related to terpenoids with high negative correlation values are found exclusively in the oil gland cells. Similarly, six flavonoids with high positive correlation were absent in the oil gland cells and present in the cells away from the glands.

Further analysis of the spectra from the oil gland cells revealed the presence of diverse chemical species tentatively identified as terpenes and modified terpenoids, including hemiterpenes, monoterpenes, and diterpenes. The large chemical diversity of these compounds and the amount of work it takes to fully characterize a species highlights the importance of the OPLS-DA-based method that enables us to pinpoint the metabolites that contribute to most of the variance between the LAESI-MS spectra of different subpopulations. These compounds can be

viewed as candidates for biomarkers, but their verification requires extensive testing, including biological assays.

CONCLUSIONS

In this article we demonstrated the feasibility of using a small population of single cells as voxels in a LAESI-MS imaging experiment. On the basis of profiling hexose and disaccharide ion intensities, we found that the microablation of a cell using a sharpened optical fiber does not significantly alter the metabolite composition of the adjacent cells. For secondary metabolites associated with pigmentation, the chemical contrast observed in the LAESI-MS images followed the visual contrast observed by optical microscopy. Producing images built from cellular voxels promises additional insight into cellular transport, localization, and signaling in biological tissues.

At present, the main limitations of cell-by-cell imaging are related to the size and number of cells used in these experiments. Because of instrument sensitivity limitations, the dimensions of the currently accessible smallest area are \sim 30 μm in diameter. Although many plant cells have larger dimensions, they often exhibit high aspect ratios, e.g., the flattened cells in this study. Currently the minimum size requirement is to be able to ablate a circular spot of 30 μm in diameter to a depth of \sim 30 μm that remains entirely within a single cell. As the efficiency of the LAESI interface improves, further reduction in the dimensions of the studied cells is expected. In particular, various cells of vertebrates with typical dimensions of \sim 10 μm may become possible.

The number of cells in the demonstrated images is very small. This obvious limitation is set by the current need to manually locate each cell targeted for analysis within the irregular cellular pattern of the tissue. A possible solution for this problem can be based on a computerized gridding algorithm, based on recognizing the cells as objects in the optical microscope image of the tissue, and generating a grid of ablation points that matches the cellular pattern. Feeding these coordinates to the motorized translation stage of the sample holder would eliminate the need to manually address the ablated cells and enable the construction of images with larger voxel counts. Because of the need to retain the water content in the sample for LAESI analysis, cell-by-cell imaging of samples with a large number of voxels requires the implementation of an environmental chamber for humidity control to prevent drying.

Local LAESI-MS analysis of \sim 30 μm diameter voxels also enables the investigation of metabolites and lipids in small cell populations. The actual size of the population depends on the average cell size. For example in the case of larger plant cells, very small populations in the $1 < n < 50$ size range can be studied, whereas in the case of smaller animal cells the population size can fall in the $10 < n < 5000$ range. Cellular heterogeneity in larger populations can be explored by comparing the analyzed cells in a tissue voxel-by-voxel or by comparing a number of small cell populations sorted by flow cytometry.

The large volume of data produced by LAESI-MS, i.e., a spectrum for every cell or small cell population with over 300 peaks per spectrum, makes it tedious to identify every metabolite in the sample. Many times, however, this is not the objective of the analysis and in these cases assignment of a much smaller subset of peaks is sufficient. For example, in the search for biomarkers, salient chemical species are sought by comparing the metabolite content of two different regions in a tissue (e.g., a

lesion with the surrounding unaffected areas) or two sets of small cell populations (e.g., a drug treated and a control).

We demonstrated the utility of OPLS-DA, a multivariate data analysis tool, for the selection of a small number of metabolites that accounted for most of the variance in LAESI-MS data of different cell subpopulations. On the basis of the preexisting information on the cells involved (e.g., nonpigmented vs pigmented epidermal cells), the results of the OPLS-DA analysis were easily verified. Finding the statistically significant differences in metabolite content, however, does not necessarily mean the discovery of true biomarkers. For the verification of each of the identified candidates, biological assays are needed. Guided by OPLS-DA analysis of LAESI-MS data, however, dramatically reduces the number of detected metabolites that needs structural identification.

■ ASSOCIATED CONTENT

Supporting Information. Additional information as noted in text. This material is available free of charge via the Internet at <http://pubs.acs.org>.

■ AUTHOR INFORMATION

Corresponding Author

*E-mail: vertes@gwu.edu. Phone: +1 (202) 994-2717. Fax: +1 (202) 994-5873.

■ ACKNOWLEDGMENT

The authors acknowledge financial support from the U.S. National Science Foundation (Grant 0719232), the U.S. Department of Energy (Grant DEFG02-01ER15129), Protea Biosciences, Inc., and the George Washington University Research Enhancement Fund. The GeO₂-based glass optical fibers used in this study were generously provided by Infrared Fiber Systems, Inc., Silver Spring, MD.

■ REFERENCES

- (1) Elowitz, M. B.; Levine, A. J.; Siggia, E. D.; Swain, P. S. *Science* **2002**, *297*, 1183.
- (2) Sigal, A.; Milo, R.; Cohen, A.; Geva-Zatorsky, N.; Klein, Y.; Liron, Y.; Rosenfeld, N.; Danon, T.; Perzov, N.; Alon, U. *Nature* **2006**, *444*, 643.
- (3) Snijder, B.; Sacher, R.; Ramo, P.; Damm, E.-M.; Liberali, P.; Pelkmans, L. *Nature* **2009**, *461*, 520.
- (4) Davey, H. M.; Kell, D. B. *Microbiol. Rev.* **1996**, *60*, 641.
- (5) Cohen, D.; Dickerson, J. A.; Whitmore, C. D.; Turner, E. H.; Palcic, M. M.; Hindsgaul, O.; Dovichi, N. J. *Annu. Rev. Anal. Chem.* **2008**, *1*, 165.
- (6) Mack, E.; Neubauer, A.; Brendel, C. *Cytometry, Part A* **2007**, *71A*, 404.
- (7) Amantonicco, A.; Urban, P. L.; Fagerer, S. R.; Balabin, R. M.; Zenobi, R. *Anal. Chem.* **2010**, *82*, 7394.
- (8) Rubakhin, S. S.; Jurchen, J. C.; Monroe, E. B.; Sweedler, J. V. *Drug Discovery Today* **2005**, *10*, 823.
- (9) McDonnell, L. A.; Heeren, R. M. A. *Mass Spectrom. Rev.* **2007**, *26*, 606.
- (10) Vertes, A.; Nemes, P.; Shrestha, B.; Barton, A.; Chen, Z.; Li, Y. *Appl. Phys. A: Mater. Sci. Process.* **2008**, *93*, 885.
- (11) Rubakhin, S. S.; Greenough, W. T.; Sweedler, J. V. *Anal. Chem.* **2003**, *75*, 5374.
- (12) Xu, B. J.; Caprioli, R. M.; Sanders, M. E.; Jensen, R. A. *J. Am. Soc. Mass Spectrom.* **2002**, *13*, 1292.
- (13) Ostrowski, S. G.; Van Bell, C. T.; Winograd, N.; Ewing, A. G. *Science* **2004**, *305*, 71.
- (14) McDonnell, L. A.; Piersma, S. R.; Altelaar, A. F. M.; Mize, T. H.; Luxembourg, S. L.; Verhaert, P. D. E. M.; Van Minnen, J.; Heeren, R. M. A. *J. Mass Spectrom.* **2005**, *40*, 160.
- (15) Kulp, K. S.; Berman, E. S. F.; Knize, M. G.; Shattuck, D. L.; Nelson, E. J.; Wu, L.; Montgomery, J. L.; Felton, J. S.; Wu, K. *J. Anal. Chem.* **2006**, *78*, 3651.
- (16) Perdian, D. C.; Sangwon, C.; Jisun, O.; Donald, S. S.; Edward, S. Y.; Young Jin, L. *Rapid Commun. Mass Spectrom.* **2010**, *24*, 1147.
- (17) Hölscher, D.; Shroff, R.; Knop, K.; Gottschaldt, M.; Crecelius, A.; Schneider, B.; Heckel, D. G.; Schubert, U. S.; Svatos, A. *Plant J.* **2009**, *60*, 907.
- (18) Cooks, R. G.; Ouyang, Z.; Takats, Z.; Wiseman, J. M. *Science* **2006**, *311*, 1566.
- (19) Harris, G. A.; Nyadong, L.; Fernandez, F. M. *Analyst* **2008**, *133*, 1297.
- (20) Chen, H.; Gamez, G.; Zenobi, R. *J. Am. Soc. Mass Spectrom.* **2009**, *20*, 1947.
- (21) Li, Y.; Shrestha, B.; Vertes, A. *Anal. Chem.* **2007**, *79*, 523.
- (22) Li, Y.; Shrestha, B.; Vertes, A. *Anal. Chem.* **2008**, *80*, 407.
- (23) Wiseman, J. M.; Ifa, D. R.; Song, Q.; Cooks, R. G. *Angew. Chem., Int. Ed.* **2006**, *45*, 7188.
- (24) Wiseman, J. M.; Ifa, D. R.; Zhu, Y.; Kissinger, C. B.; Manicke, N. E.; Kissinger, P. T.; Cooks, R. G. *Proc. Natl. Acad. Sci. U.S.A.* **2008**, *105*, 18120.
- (25) Lee Chuin, C.; Kentaro, Y.; Zhan, Y.; Rikiya, I.; Hajime, I.; Hiroaki, S.; Kunihiko, M.; Osamu, A.; Sen, T.; Takeo, K.; Kenzo, H. *J. Mass Spectrom.* **2009**, *44*, 1469.
- (26) Nemes, P.; Woods, A. S.; Vertes, A. *Anal. Chem.* **2010**, *82*, 982.
- (27) Nemes, P.; Barton, A. A.; Li, Y.; Vertes, A. *Anal. Chem.* **2008**, *80*, 4575.
- (28) Nemes, P.; Barton, A. A.; Vertes, A. *Anal. Chem.* **2009**, *81*, 6668.
- (29) Nemes, P.; Vertes, A. *Anal. Chem.* **2007**, *79*, 8098.
- (30) Apitz, I.; Vogel, A. *Appl. Phys. A: Mater. Sci. Process.* **2005**, *81*, 329.
- (31) Chen, Z.; Bogaerts, A.; Vertes, A. *Appl. Phys. Lett.* **2006**, *89*, 041503.
- (32) Chen, Z. Y.; Vertes, A. *Phys. Rev. E* **2008**, *77*, 036316.
- (33) Rezenom, Y. H.; Dong, J.; Murray, K. K. *Analyst* **2008**, *133*, 226.
- (34) Sampson, J. S.; Murray, K. K.; Muddiman, D. C. *J. Am. Soc. Mass Spectrom.* **2009**, *20*, 667.
- (35) Peng, I. X.; Loo, R. R. O.; Margalith, E.; Little, M. W.; Loo, J. A. *Analyst* **2010**, *135*, 767.
- (36) Shrestha, B.; Vertes, A. *Anal. Chem.* **2009**, *81*, 8265.
- (37) Shrestha, B.; Nemes, P.; Vertes, A. *Appl. Phys. A: Mater. Sci. Process.* **2010**, *101*, 121.
- (38) Shrestha, B.; Vertes, A. *J. Vis. Exp.* **2010**, *43*, <http://www.jove.com/index/details.stp?id=2144>, DOI: 10.3791/2144.
- (39) Trygg, J.; Holmes, E.; Lundstedt, T. *J. Proteome Res.* **2006**, *6*, 469.
- (40) Miura, D.; Fujimura, Y.; Tachibana, H.; Wariishi, H. *Anal. Chem.* **2009**, *82*, 498.
- (41) Wiklund, S.; Johansson, E.; Sjostrom, L.; Mellerowicz, E. J.; Edlund, U.; Shockcor, J. P.; Gottfries, J.; Moritz, T.; Trygg, J. *Anal. Chem.* **2008**, *80*, 115.
- (42) Jolliffe, I. T. *Principal Component Analysis*; Springer Verlag: New York, 2002.
- (43) Trygg, J.; Wold, S. *J. Chemom.* **2002**, *16*, 119.
- (44) Stenlund, H.; Gorzsas, A.; Persson, P.; Sundberg, B.; Trygg, J. *Anal. Chem.* **2008**, *80*, 6898.
- (45) Nemes, P.; Marginean, I.; Vertes, A. *Anal. Chem.* **2007**, *79*, 3105.
- (46) Noda, I. *J. Mol. Struct.* **2008**, *883*, 216.
- (47) Major, H. J.; Williams, R.; Wilson, A. J.; Wilson, I. D. *Rapid Commun. Mass Spectrom.* **2006**, *20*, 3295.
- (48) Bruce, S. J.; Jonsson, P.; Antti, H.; Cloarec, O.; Trygg, J.; Marklund, S. L.; Moritz, T. *Anal. Biochem.* **2008**, *372*, 237.

- (49) Chan, E. C. Y.; Koh, P. K.; Mal, M.; Cheah, P. Y.; Eu, K. W.; Backshall, A.; Cavill, R.; Nicholson, J. K.; Keun, H. C. *J. Proteome Res.* **2009**, *8*, 352.
- (50) Trygg, J.; Holmes, E.; Lundstedt, T. *J. Proteome Res.* **2007**, *6*, 469.
- (51) Ku, K. M.; Choi, J. N.; Kim, J.; Kim, J. K.; Yoo, L. G.; Lee, S. J.; Hong, Y. S.; Lee, C. H. *J. Agric. Food Chem.* **2010**, *58*, 418.
- (52) Wilson, R. H.; Smith, A. C.; Kacurakova, M.; Saunders, P. K.; Wellner, N.; Waldron, K. W. *Plant Physiol.* **2000**, *124*, 397.
- (53) Thomson, W. W.; Platt-Aloia, K. A.; Anton, G. E. *Bot. Gaz.* **1976**, *137*, 330.
- (54) Patt, J. M.; Sétamou, M. *Environ. Entomol.* **2010**, *39*, 618.

Supporting Information for

In Situ Cell-by-Cell Imaging and Analysis of Small Cell Populations by Mass Spectrometry

Bindesh Shrestha¹, Joseph M. Patt², and Akos Vertes^{1}*

¹Department of Chemistry, W. M. Keck Institute for Proteomics Technology and Applications,
The George Washington University, Washington, District of Columbia 20052

²Beneficial Insects Research Unit, USDA Agricultural Research Service

Subtropical Agricultural Research Center, Weslaco, TX 78596

* To whom correspondence should be addressed. E-mail: vertes@gwu.edu. Phone: +1 (202) 994-2717.
Fax: +1 (202) 994-5873.

Table S1. Typical instrumental parameters for the cell-by-cell LAESI-MS imaging experiment.

Parameter	Value
Electrospray emitter	Stainless steel; i.d., 50 μm
Electrospray voltage	2.9 to 3.0 kV
Solution supply rate	200 nL/min
Solvent composition	50% (v/v) aqueous methanol with 0.1% (v/v) acetic acid
Laser wavelength and pulse width	2940 μm and 5ns
Laser pulse repetition rate	10 Hz
Laser pulse energy before coupling to fiber	0.55±0.03 mJ
Optical fiber	GeO ₂ -based glass fiber, 450 μm core diameter
Coupling lens for optical fiber	planoconvex CaF ₂ lens with 50.0 mm focal length
MS orifice temperature	80 °C
MS acquisition mode	Positive ions
MS orifice-to-emitter tip distance	12 mm
MS orifice axis-to-sample surface distance	12 mm
Dwell time between pixels	60 s

Table S2. Analyzing the single cell LAESI-MS spectra of pigmented and colorless cells with OPLS-DA identified 7 metabolites as candidates for biomarkers of the pigmented cell type. Based on the S-plot in Figure 3b, the metabolites marked with serial numbers (SN) were responsible for most of the variance between pigmented (purple background) and colorless (white background) cell spectra.

SN	Metabolite	Ion	<i>m/z</i>
1	cyanidin	C ₁₅ H ₁₁ O ₆ ⁺	287.0551
2	quercetin*	C ₁₅ H ₁₀ O ₇ (+H ⁺)	303.0498
3	cyanidin malonyl glucoside*	C ₂₄ H ₂₃ O ₁₄ ⁺	535.1110
4	quercetin glucoside*	C ₂₁ H ₂₀ O ₁₂ (+H ⁺)	465.1027
5	quercetin diglucoside*	C ₂₇ H ₃₀ O ₁₇ (+Na ⁺)	649.1414
6	quercetin diglucoside*	C ₂₇ H ₃₀ O ₁₇ (+H ⁺)	627.1561
7	disaccharide	C ₁₂ H ₂₂ O ₁₁ (+H ₂ O+K ⁺ +H ⁺)	200.0439
8	hexose dimer	(C ₆ H ₁₂ O ₆) ₂ (+Na ⁺)	383.1135
9	disaccharide	C ₁₂ H ₂₂ O ₁₁ (+K ⁺)	381.0799
10	hexose	C ₆ H ₁₂ O ₆ (+Na ⁺)	203.0560
11	hexose	C ₆ H ₁₂ O ₆ (+K ⁺)	219.0285

*Identification was aided by tandem MS.

Table S3. Analyzing the LAESI-MS spectra of highly dissimilar buccal epithelial and *A. cepa* epidermal cells selected by OPLS-DA identified 10 metabolites that, according to the S-plot in Figure S2b, were responsible for most of the variance between the spectra of buccal epithelial (**SN = 1, 2, 3**) (white background) and *A. cepa* cells (**SN > 3**) (yellow background).

SN	Metabolites	Ion	m/z
1	DG (36:4)	C ₃₉ H ₆₈ O ₅ (+H ⁺)	617.5155
2	MG (18:2)	C ₂₁ H ₃₈ O ₄ (+H ⁺)	355.2840
3	DG (33:3)	C ₃₆ H ₆₄ O ₅ (+Na ⁺)	599.4783
4	oligosaccharide (5 hexose units)	C ₃₀ H ₅₂ O ₂₆ (+K ⁺ +H ⁺)	434.1201
5	disaccharide (2 hexose units)	C ₁₂ H ₂₂ O ₁₁ (+H ₂ O+K ⁺ +H ⁺)	200.0448
6	oligosaccharide (6 hexose units)	C ₃₆ H ₆₂ O ₃₁ (+H ₂ O+K ⁺ +H ⁺)	524.1516
7	oligosaccharide (5 hexose units)	C ₃₀ H ₅₂ O ₂₆ (+H ₂ O+K ⁺ +H ⁺)	443.1234
8	disaccharide (2 hexose units)	C ₁₂ H ₂₂ O ₁₁ (+K ⁺)	381.0773
9	trisaccharide (3 hexose units)	C ₁₈ H ₃₂ O ₁₆ (+K ⁺)	543.1285
10	hexose	C ₆ H ₁₂ O ₆ (+K ⁺)	219.0228

Table S4. Biomarker candidate metabolites identified by OPLS-DA analysis of spectra produced by LAESI-MS from small cell populations in an oil gland of a *C. aurantium* leaf (**SN = 1, 2, 3, 4**) (white background) and in tissue away from the gland (**SN > 4**) (green background). Based on the S-plot in Figure 5b, they are responsible for most of the variance between the spectra of cells in the oil gland and tissue away from the oil gland.

SN	Metabolite	Ion	m/z
1	monoterpene*	C ₁₀ H ₁₆ (+H ⁺)	137.1330
2	monoterpene fragment	C ₆ H ₉ ⁺	81.0708
3	citral and/or pulegone	C ₁₀ H ₁₆ O (+H ⁺)	153.1308
4	cymene	C ₁₀ H ₁₄ (+H ⁺)	135.1180
5	hesperetin	C ₁₆ H ₁₄ O ₆ (+H ⁺)	303.0780
6	rhamnocitrin rhamnoside	C ₃₄ H ₄₂ O ₁₉ (+H ⁺)	755.2497
7	peonidin glucoside	C ₂₂ H ₂₃ O ₁₁ ⁺	463.1180
8	methylkaempferol*	C ₁₆ H ₁₃ O ₆ ⁺	301.0721
9	kaempferol rhamnoside glucoside*	C ₂₇ H ₃₀ O ₁₅ (+H ⁺)	595.1631
10	diosmin or cytisoside-O-glucoside	C ₂₈ H ₃₂ O ₁₅ (+H ⁺)	609.1827

*Identification was aided by tandem MS.

Figure S1. (a) Optical microscope image of the *A. cepa* tissue at a transition region between colorless and purple cells. Cell-by-cell chemical images of the metabolites (b) quercetin, and (c) alliin were created by representing the ion intensities obtained from a cell on a false color scale and coloring the corresponding cells in the microscope image accordingly.

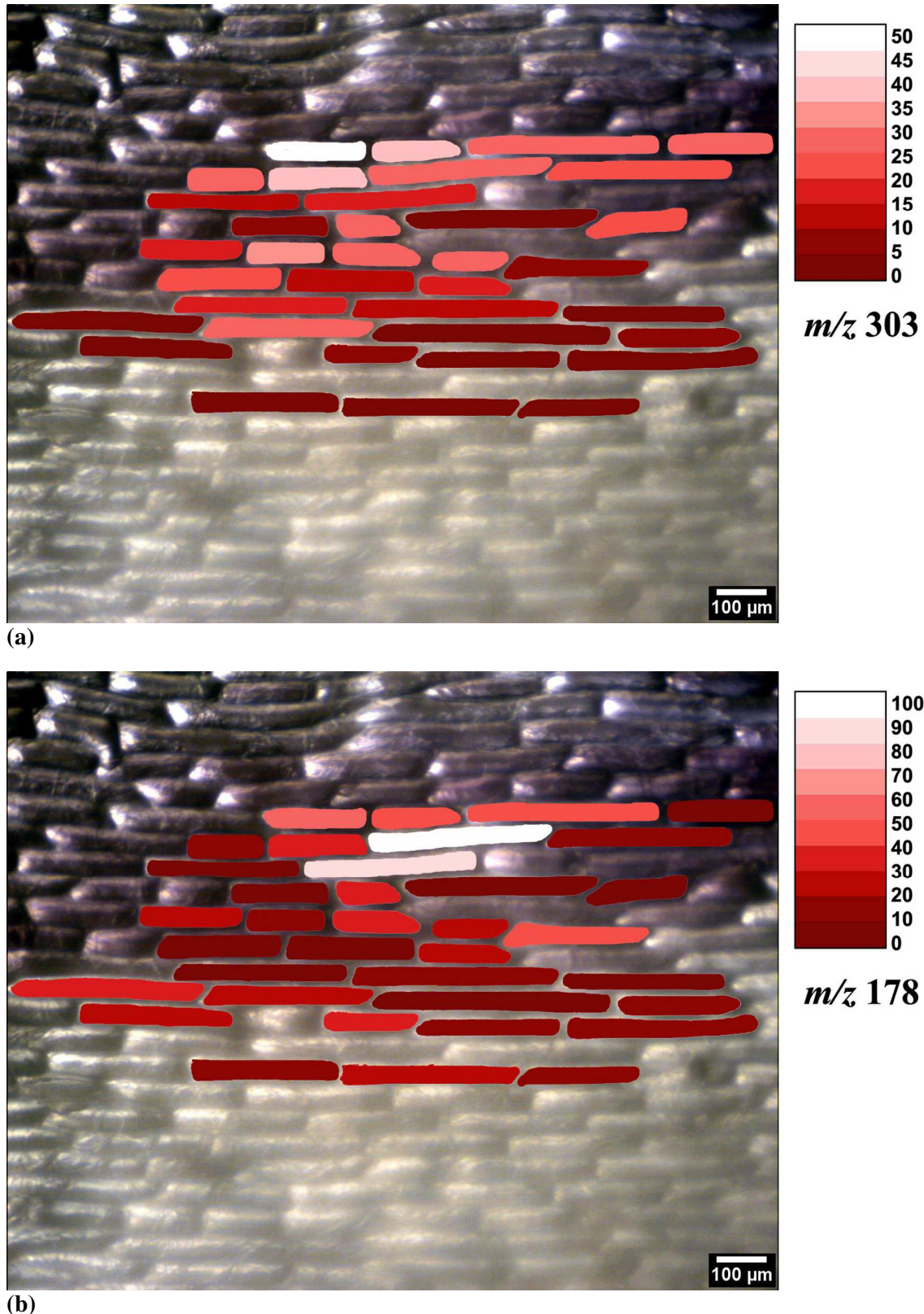
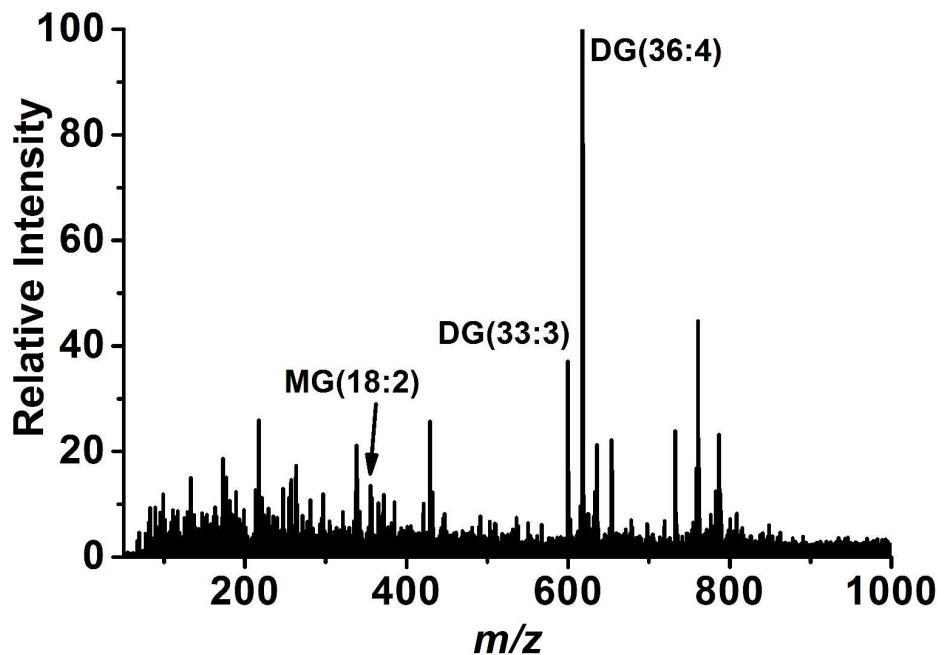
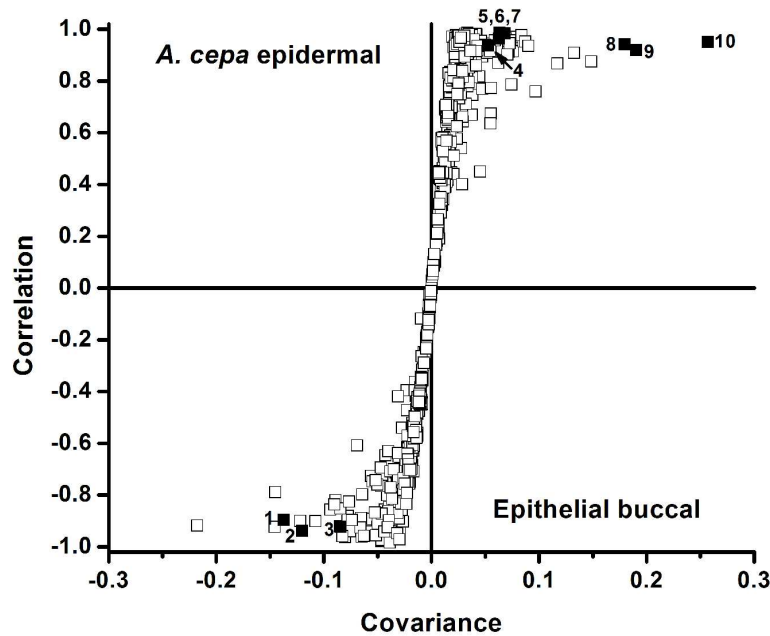


Figure S2. (a) Positive-ion LAESI mass spectra of approximately six human buccal epithelial cells ($n = 6$) showed the presence of small metabolites and lipids. (b) Comparison of LAESI mass spectra of highly dissimilar buccal ($n = 18$) and *A. cepa* ($n = 9$) cell populations by OPLS-DA resulted in an S-plot that spanned the entire -1 to 1 correlation range. Metabolites with high correlation and covariance values were exclusively present in spectra of the two cell types. Some of them (solid squares) were identified by serial numbers and listed in Table S2.

(a)



(b)



ACKNOWLEDGMENTS

The authors acknowledge financial support from the U.S. National Science Foundation (Grant 0719232), the U.S. Department of Energy (Grant DEFG02-01ER15129), Protea Biosciences, Inc., and the George Washington University Research Enhancement Fund. The GeO₂-based glass optical fibers used in this study were generously provided by Infrared Fiber Systems, Inc., Silver Spring, MD.